Remote sensing techniques applied to geomorphological mapping of rocky coast: the case study of Gallinara Island (Western Liguria, Italy)

Bianca Federici, Nicola Corradi, Ilaria Ferrando, Domenico Sguerso, Antonio Lucarelli, Sara Guida & Pierluigi Brandolini

Published online: 18 Nov 2019.

Submit your article to this journal

Article views: 119

View related articles

View Crossmark data

Taylor & Francis
Taylor & Francis Group

Remote sensing techniques applied to geomorphological mapping of rocky coast: the case study of Gallinara Island (Western Liguria, Italy)

Bianca Federici [a], Nicola Corradi [b,c], Ilaria Ferrando [a], Domenico Sguerso [a], Antonio Lucarelli[d], Sara Guida[b] and Pierluigi Brandolini [b]

[a]DICCA, Department of Civil, Chemical and Environmental Engineering, University of Genoa, Genoa, Italy; [b]DISTAV, Department of Earth, Environment and Life Sciences, University of Genoa, Genoa, Italy; [c]GNRAC, National Research Group for Coastal Environment, Genoa, Italy; [d]DSS, Drafin Sub Survey, Genoa, Italy

ABSTRACT

Geomorphological survey and mapping of the emerged and submerged coastal areas, particularly addressed to evaluate sea cliff instability within the assessment of coastal hazard and risk mitigation measures, require high resolution and georeferenced spatial data. Remote sensing techniques fully satisfy these needs and allow to obtain all information in a single short-lived survey campaign. An integrated survey by means of laser scanner and multibeam techniques coupled with aerial photos interpretation has been experienced along the rocky coast of the Gallinara Island (Western Liguria, Italy). The small extent of Gallinara, together with its particular meteo-marine climate conditions, makes the island a noteworthy case study. Multibeam and laser scanner technologies allowed to reconstruct the submerged and emerged rocky coast at high resolution. The accuracy of the 3D surface reconstructed by means of laser scanner used in profiler mode was tested and validated, by comparing with the static laser scanner survey method. The resulting data allowed to obtain significant geological and geomorphological information leading to the definition of rocky cliff stability conditions.

Introduction

The rapid technological evolution of remote sensing survey techniques has led many researches to focus on their integration and on the management and elaboration of the huge amount of resulting data (point clouds and Digital Terrain/Surface Models). Survey techniques, such as static or mobile laser scanner, terrestrial or UAV (Unmanned Aerial Vehicles) photogrammetry and multibeam, are nowadays applied to various fields, from the analysis of terrestrial, marine or fluvial environments, to urban areas and cultural heritage. At present, the main objective is to achieve the necessary precision and resolution together with ensuring a reasonable use of resources and time (Gagliolo et al., 2018; Nex & Remondino, 2014; Passoni, Federici, Ferrando, Gagliolo, & Sguerso, 2018). Hence, optimized survey planning and realization, coupled with well-thought processing, allow to obtain high-quality results. This attention was posed by the authors during the application introduced in the following.

Laser scanner and multibeam integration is widely applied to support geo-hydrological risk mitigation measures assessment and land management in coastal or fluvial areas (Alho et al., 2009; Aguilar et al., 2017; Boeder, Kersten, Hesse, Thies, & Sauer, 2010, 2015; Brandolini, Faccini, Robbiano, & Terranova, 2009;

Capra et al., 2017; Colbo, Ross, Brown, & Weber, 2014; Del Monte et al., 2015; Ferrari et al., 2019; Mancini et al., 2013; Mills, Buckley, Mitchell, Clarke, & Edwards, 2005; Monteys, Harris, Caloca, & Cahalane, 2015; Pranzini & Williams, 2013; Raso, Brandolini, Faccini, & Firpo, 2016; Raso et al., 2017; Troisi, Del Pizzo, Gaglione, Miccio, & Testa, 2015). Investigations on the stability of rocky coasts have often been carried out using such remote sensing techniques (Naylor, Stephenson, & Trenhaile, 2010), both for monitoring erosion of hard rock coastal cliffs (Rosser, Petley, Lim, Dunning, & Allison, 2005), and for detailed mapping of rock-failure susceptibility by means of non-contact geo-structural surveys (De Vita, Cevasco, & Cavallo, 2012). In fact, in the framework of rocky coastal environment, where it is necessary to get detailed georeferenced data both at sea and inland, remote sensing techniques allow the acquisition of the whole information in a single and integrated survey campaign.

In this context, an integrated survey of the rocky coast and sea bottom of Gallinara Island (Western Liguria, Italy), by coupling laser scanner and multibeam techniques with aerial photos interpretation, was carried out with the aim to produce a Digital Terrain Model (DTM) both of the emerged and submerged coastal zone.

Gallinara is a small island with an extent of 0.11 km^2 and a maximum elevation of 87 m a.s.l. (Figure 1); it is
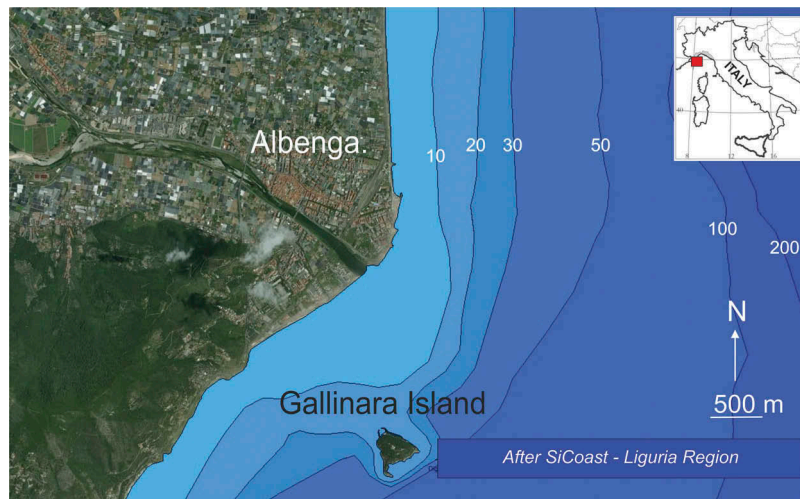
Figure 1. Location of the study area.

included in a Regional park since 1989. The island is mainly characterized by the cropping out of quartzites and secondly by conglomerates belonging to the "Quarziti of Monte Bignone" Formation (Upper Cretaceous). Its small extent and peculiar meteo-marine climate conditions make the Gallinara Island a noteworthy case study (Guida, Corradi, Federici, Lucarelli, & Brandolini, 2019).

In order to guarantee the quality of the obtained results, remote sensing techniques applied to coastal geomorphological investigations were tested and validated, by comparing static and kinematic laser scanner survey methods. Hence, the Digital Surface Model (DSM) derived by the point clouds elaboration allowed to obtain remarkable geological and geomorphological information, which can be useful for the evaluation of susceptibility to instability of the sea cliffs (Brandolini et al., 2018; Caputo et al., 2018; Cevasco, Pepe, & Brandolini, 2013; Faccini, Brandolini, Robbiano, Perasso, & Sola, 2005; Scarpati, Pepe, Mucerino, Brandolini, & Firpo, 2013).

Materials and methods

Integrated remote sensing survey

The remote sensing survey of the rocky cliffs and sea bottom of the Gallinara Island has been carried out in 2 days, mainly circumnavigating the island with a properly equipped boat. The island is a private property, except for the refuge port, thus the direct access was forbidden.

The boat was equipped by the Teledyne Reson PDS2000 platform, for the simultaneous acquisition of a MultiBeam EchoSounder (MBES) R2Sonic 2024 (Brennan, 2009), a Sound Velocity Profiler (SVP) RESON mod. SVP-15, an Inertial Measurement Unit (IMU) IXBLUE mod. HYDRINS III, a Laser Scanner (LS) RIEGL mod. LMS-Z420i (RIEGL GmbH, 2010) used in profiler mode, and a GPS 5700 TRIMBLE
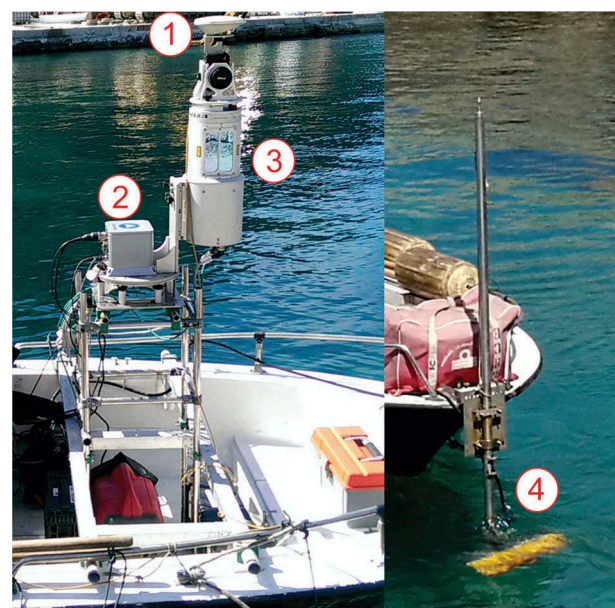
Figure 2. On board technical equipment (see the text for acronyms): 1) GPS-RTK; 2) IMU; 3) LS; 4) MBES.

receiver in "rover" Real-Time Kinematic configuration(GPS-RTK) (Figure 2).

A second GPS 5700 TRIMBLE receiver was used in static configuration on three cornerstones on the coast and one in the refuge port of the island (P3 in Figure 3), to get the absolute coordinates to be associated to the point cloud of the cliffs surveyed by boat. Hence, it was left on the cornerstone in the refuge port and connected via radio to the "rover" GPS receiver on the boat acquisition platform, working as "base" to georeference the boat in relative.

Moreover, a GPS RTK kinematic survey was performed along transects in the area characterized by low water depth inside the refuge port, where the boat was not able to enter (Figure 3).

A static LS survey has been performed in the refuge port from three different positions (ST 1–3 in Figure 4). Three reflective cylindrical targets of 0.1 m diameter

Figure 3. Cornerstone (P3) on the dock of the refuge port where GPS static survey was performed; the red rectangle indicates the area surveyed by kinematic GPS along transects, due to the low water depth.
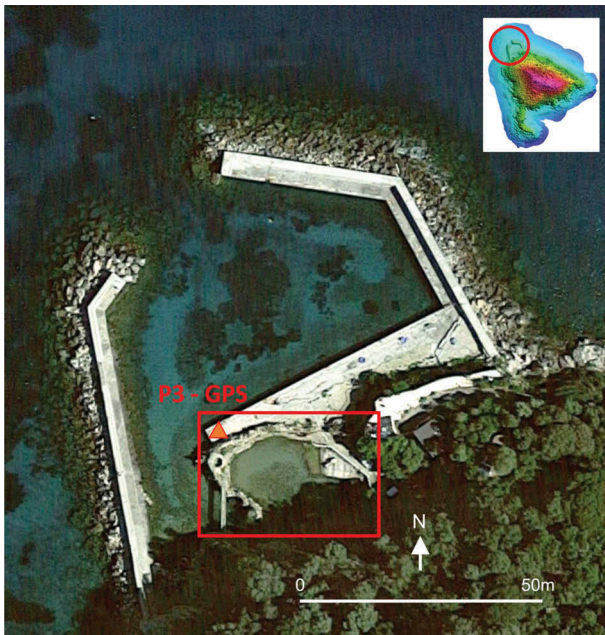
(R1-1, R1-2 and R1-3 in Figure 4) and one of 0.3 m diameter (R2 in Figure 4) were placed on the protective piers in addition to natural or anthropogenic targets, to improve the accuracy in the cloud registration phase. Their position was surveyed by GPS RTK positioning.

Static LS was also integrated with a camera to associate the color to the resulting point cloud.

The profiler mode (hereafter kinematic) LS survey, performed from the boat, was calibrated acquiring

parts of the refuge port, by means of a series of pre-established routes, so to detect the reflective cylinder R2 from different positions, angles and distances, as well as different natural or anthropogenic reference points. Hence, the comparison with the static point cloud, considered as reference, helped in evaluating the mechanical errors in the installation of instruments on the boat and compensating the profiler point cloud.

The RIEGL mod. LMS-Z420i instrument, used both in static and profiler mode, is characterized by 1 km maximum range and a repeatability of 8 mm on a single measurement and 4 mm on average, that allowed to reach a precision of the order of 1 cm during the static survey in the refuge port. In profiler mode, precision varies between 3 and 5 cm, depending on the angular precision of IMU and the distance from the cliff. A careful comparison between static and kinematic LS data in the refuge port area, is detailed in the following (see par. 3.1), to enhance the precision and quality of the resulting point clouds.

The MultiBeam EchoSounder (MBES) R2Sonic 2024 instrument is characterized by a 256 beams of 0.5° × 1° beam width across and along track at 450 kHz. In order to investigate the portions of the bottom close to the free surface, the multibeam was mounted on a joint angled at 30°, thus physically tilting the transducer to exploit the entire swath of the MBES.

The MBES system required a preventive calibration phase both for the synchronization of the timescale of each instrument (IMU, MBES, LS) with respect to GPS time and for the compensation of the Roll, Pitch and Yaw angles due to the mechanical assembly of the system with respect to the ideal configuration. An
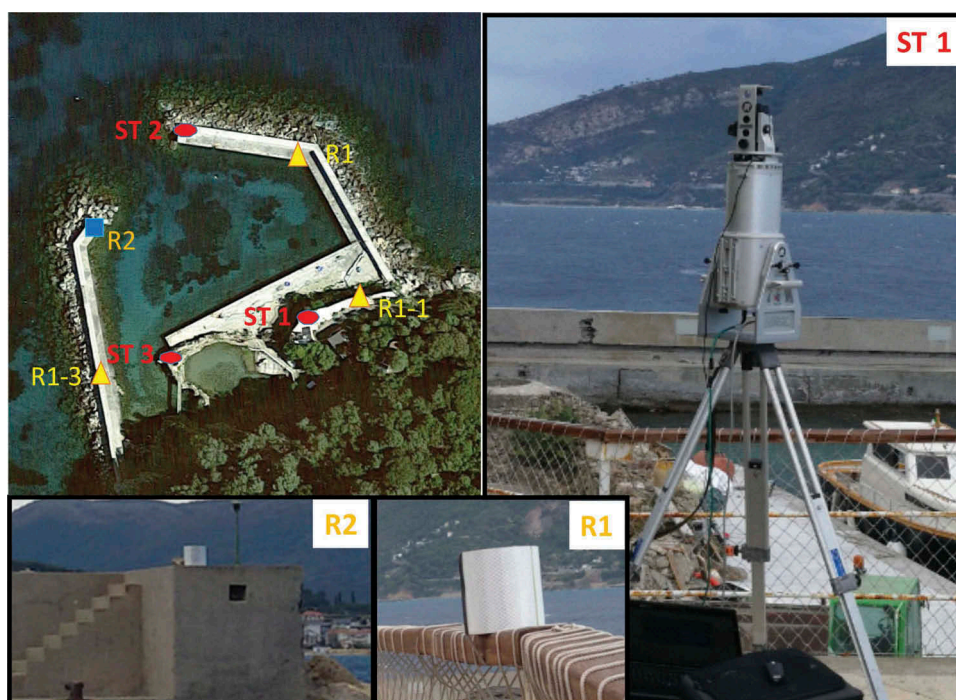

Figure 4. Example of static LS survey and reflective cylinders and their relative position in the refuge port.

analogous (exclusively) manual calibration procedure was necessary for the correction of the Roll, Pitch and Yaw parameters of the kinematic LS too.

The MBES control interface allows data filtering, which is essential for both automatically removing noise in water (caused by navigation motion), and helping the operator during surface filtering (despiking), removing the background noise (spikes). It is recommended to employ an experienced operator to (manually) perform the despiking, especially in presence of articulated geological structures.

Sea bottom MBES, processed by the platform Teledyne Reson PDS2000, allowed to obtain a detailed submerged DSM with 0.25 × 0.25 m resolution. The static LS data, processed with the software Riscan Pro by Riegl, and the kinematic LS data, processed by the platform Teledyne Reson PDS2000, allowed to describe the emerged rocky coast at 2–4 cm resolution.

The final result was the reconstruction of a continuous 3D model both for emerged and submerged coastal areas (Figure 5), that allows to obtain significant geological and geomorphological data of the site.

Geomorphological coastal susceptibility mapping

Following the official guidelines of the geomorphological legend published by the former National Geological Service (now ISPRA, Italian Institute for the Environmental Protection and Research) in collaboration with the National Working Groups of the Italian Association of Physical Geography and Geomorphology (AIGeo), a geomorphological sketch map has been produced by aerial photos interpretation supported by the obtained 3D model and by observations from boat (Campobasso et al., 2018; Chelli et al., 2018; Mastronuzzi et al., 2017).

To define the geomorphological landslide susceptibility along the coastal perimeter of the Gallinara Island, a laser scanner survey has been carried out in five sectors representative of the prevailing rocky cliffs conditions and sea bottom morphology (Figure 5). The obtained high-resolution DTM allowed to measure the attitude of the bedding surfaces and of the other main morphological and structural features of the bedrock (useful for the application of the "Sea Cliff Mass Rating" (SCMR) classification.

The SCMR is a rock mass classification method, which is widely adopted on rocky cliffs to evaluate their quality and degree of stability, expressed by means of the index defined in the following equation:

$$SCMR = R1 + R2 + R3 + R4 + R5 + (F1 \cdot F2 \cdot F3) + F4m - M \tag{1}$$

According to Lucchetti et al. (2014), R1, R2, R3, R4, R5 are the parameters after the RMR rock mass classification by Bieniawski (1989); F1, F2 e F3 are part of the parameters after the SMR classification by Romana (1993); F4m is a parameter that considers any consolidation works carried out on the cliff. The parameter M introduces the sea wave action deriving from the sum of three parameters:

- M1 takes into consideration how the sea waves reach the rock wall (broken or breaking waves) and the sea wave energy, evaluated with the relation

$$E = \frac{1}{8}\rho \cdot g \cdot H_s^2 \tag{2}$$

- M2 is a function of the inclination α of the cliff: if the scarp is vertical, sea waves transmit the maximum energy to the cliff, therefore the pressure applied by the sea waves is directly proportional to the angle α;
- M3 is defined by the angle θ formed between the sea waves direction and the coastline, considering that when the sea wave hit perpendicularly the coast line, it discharges the higher pressure on the cliff face.
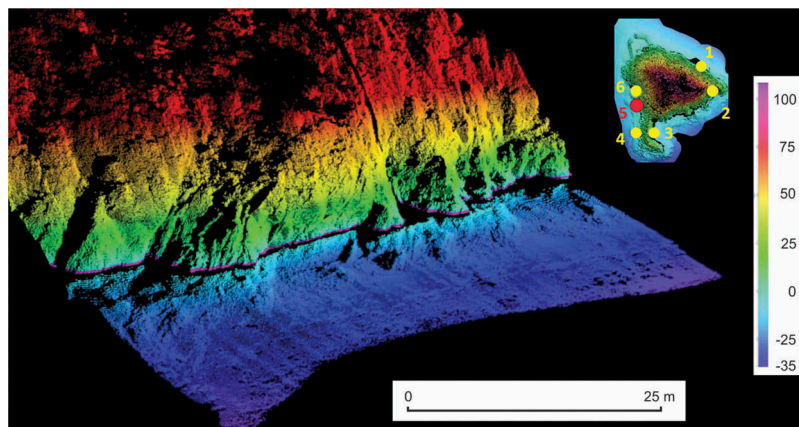

Figure 5. Example of point clouds continuity between multibeam and laser scanner integrated survey, representing both of the emerged and submerged sea cliff. It refers to the position indicated with a red dot in the Gallinara island in the right-up corner; the yellow dots represents the positions of the other 5 portions of cliff analysed.

The SCMR classification identifies five classes of cliff quality (Table 1) on the basis of the values attributed to the various parameters, as showed in Lucchetti et al. (2014).

In order to identify also the morphology of the sea bottom, the topographic profiles of both emerged and submerged cliff have been reconstructed for each test station (which positions are reported in Figure 5), deploying the DTM obtained by the integration of laser scanner and multibeam surveys.

Finally, a susceptibility map of coastal instability, based on the correlation between SCMR and geomorphological data, has been produced according to the method proposed by Lucchetti et al. (2014). This method identifies five Susceptibility Coastal Instability (SCI) classes. Moreover, a sixth class, defined as "techno-coast", has been added to represent the harbor works and others man-made interventions that have completely covered the sea cliff.

Results

Focus on laser scanner quality

The static (performed on land) and kinematic (performed from the boat) point clouds have been compared in their overlapping area, namely the refuge port, to assess their quality. The comparison and the following elaborations have been performed using the free and open-source software CloudCompare, ver. 2.10 (2019).

The static and kinematic clouds in the port area are constituted by about 6.2 million and 2.7 million points, respectively. A rough estimate of the overlapping area has been carried out, separating the portions belonging only to the static and kinematic point clouds. To pursue this goal, a constant field has been added to each point

cloud, with value 1 for static and 10 for kinematic, respectively. Then, the point clouds have been merged and sampled in 10×10 cm cells, using the Rasterize tool in CloudCompare. The average value of the constant field has been assigned to each cell, on the basis of the values of points falling in it. Finally, the resulting point cloud has been filtered according to the value of each cell: the cells with a mean value of 1 have been classified as only static, the cells with a mean value of 10 have been classified as only kinematic, the cells with mean values between 1.01 and 9.99 have been classified as both static and kinematic. The results of this operation are reported in Figure 6, where the only static, only kinematic and both static and kinematic areas are represented in red, green and blue, respectively. Table 2 reports the number of points for each portion and the corresponding percentage.

A DSM has been computed from each static and kinematic point cloud, sampling in 10×10 cm cells and assigning at each cell the average value of the height of the points falling in it. The resulting DSMs are reported in Figure 7. Note that both DSMs have cells with a height lower than the sea level, until 40 cm below, being the LS technology able to survey shallow-water depth.

The static and kinematic resulting DSMs are constituted by about 230,000 and 295,000 cells, respectively. The total number of cells of a DSM does not depend on the number of points in the point cloud, but on its spatial extension; thus, it is evident that the kinematic point cloud covers a larger area than the static one, even if described by less surveyed points.

The generated DSMs give useful information for each cell, which can be employed to characterize the point cloud. Among them, the per-cell population and the height standard deviation of each cell have been considered for the two point clouds.
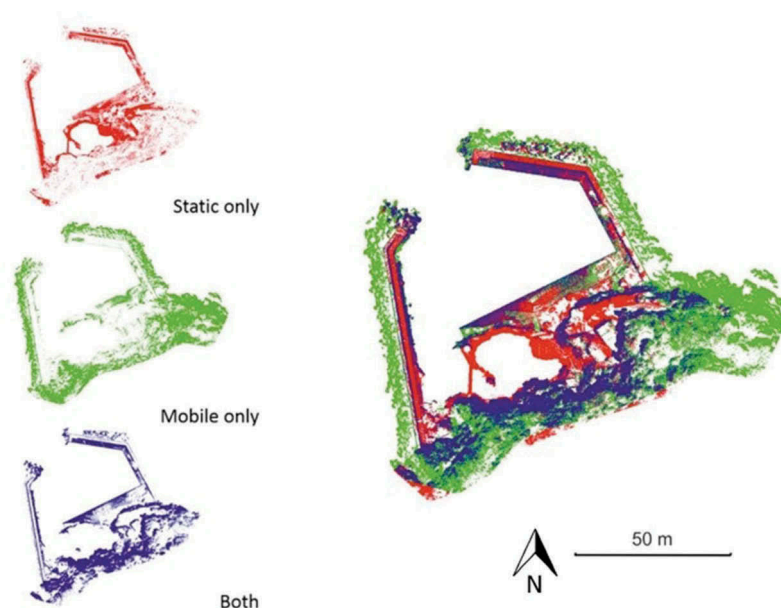

Figure 6. Static only, kinematic only and both static and kinematic surveyed areas represented in red, green and blue, respectively.

Table 1. Rock mass quality classes of seacliffs based on SCMR Classification (after Lucchetti et al., 2014).

SCMR	100–81	80–61	60–41	40–21	20–0
Class	I	II	III	IV	V
Description	Very good	Good	Fair	Poor	Very poor
Stability	Completely stable	Stable	Partially stable	Unstable	Completely unstable
Type of failure	None	Some blocks	Some joints or many wedges	Planar or big wedges	Big planar or toppling
Stabilization	None	Occasional	Systematic	Important	Re-excavation

Table 2. Number of points and the corresponding percentage of surface surveyed with only static or kinematic LS and over-lapping areas.

Portion	Number of points	Percentage
Only static	92,580	23.86%
Only kinematic	157,263	40.54%
Overlapping area	138,129	35.60%

The per-cell population represents the number of points falling in a cell of given dimensions (10 × 10 cm in the present case); thus, it can give a rough indication of point cloud density. The static DSM has a higher average value of per-cell population (equal to 27) and a higher standard deviations of the per-cell population (equal to 170) with respect of the kinematic one (average value equal to 9 and standard deviation of 23). The high value of average per-cell population of the static LS DSM is a consequence of a denser original point cloud. Observing Figure 8, a higher density results near the scanning stations in the static DSM, while the kinematic DSM results denser along the protective piers.

The heights standard deviations parameter measures the dispersion of height values inside each cell: the smaller is its value, the more homogeneous are the points heights. It results that the two DSMs have very low and similar values of height standard deviation (average value equal to 0.29 m and 0.34 m and standard deviation equal to 0.61 m and 0.60 m for static and kinematic DSMs, respectively), showing a substantial homogeneous distribution of heights in the point clouds. As expected, the higher values of height standard deviation are mainly located in areas covered with vegetation, where the point clouds result

noisier and characterized by large differences in height between ground and trees (Figure 9).

Finally, the two DSMs have been compared concerning the average height value in each cell. This has been done deploying the CloudCompare's M3C2 plug-in (Lague, Brodu, & Leroux, 2013), which allows to obtain signed distances between two points clouds. The result is shown in Figure 10, obviously only on the overlapping area of the two DSMs. The average value and standard deviation of the differences (static – kinematic) are 0.19 m and 0.86 m. Again, the higher differences are located in vegetated areas, while elsewhere the two point clouds are very similar.

In order to quantify the quality of the kinematic survey with respect to the static one, the differences in height have been also computed in three selected portions of the DSMs, depending on the type of surface, e.g. anthropogenic area, bare rock and vegetated area. The chosen study areas are: the concrete piers and the docking area, a portion of a rocky cliff and an area covered by vegetation, as illustrated in Figure 11 in yellow, green and blue colors, respectively.

The M3C2 algorithm, applied to each area separately, has enhanced the average values and standard deviations of the differences (static – kinematic) reported in Table 3. The different areas have similar average values of differences in absolute value (the exception is the negative sign of differences for piers and dock portion), while the vegetated area has a higher standard deviation, as expected. Concerning the piers, the higher differences are mainly located along the external edges, and are probably due to the highly inclined view of the static survey, which reduces the quality and the reliability of the survey itself.
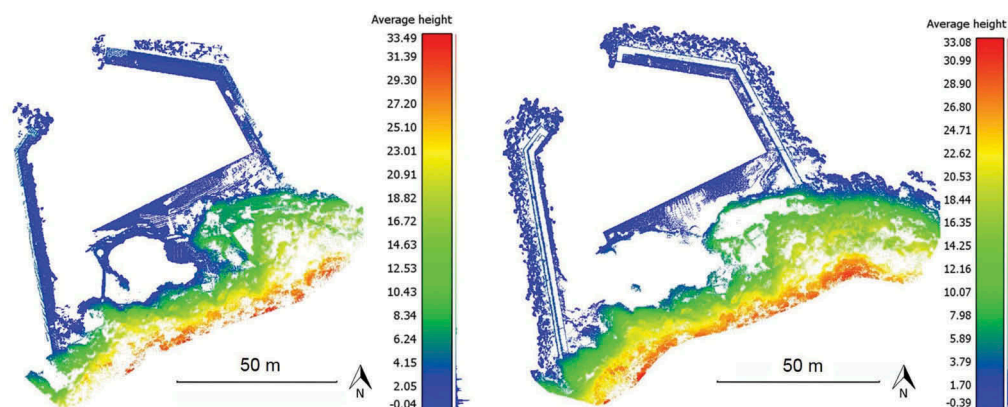
Figure 7. Static (left) and kinematic (right) DSMs and statistical distribution of height values (next to the scale bars).
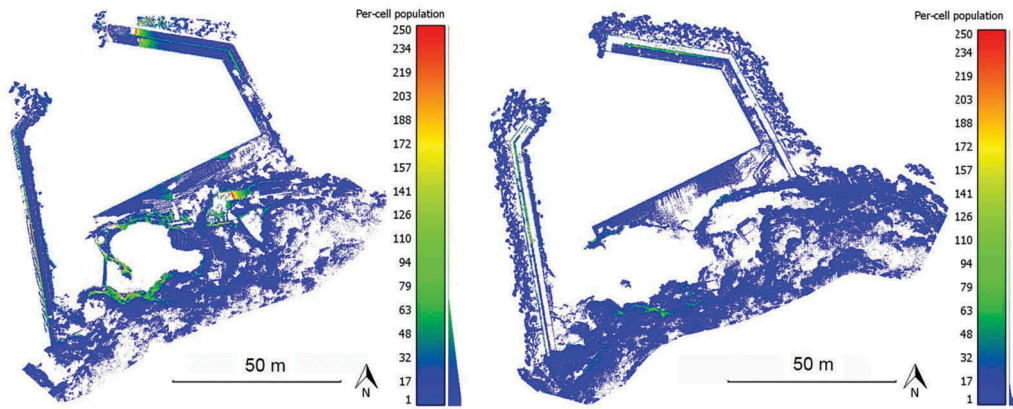
Figure 8. Per-cell population for static (left) and kinematic (right) DSMs, and statistical distribution of the values (next to the scale bars).
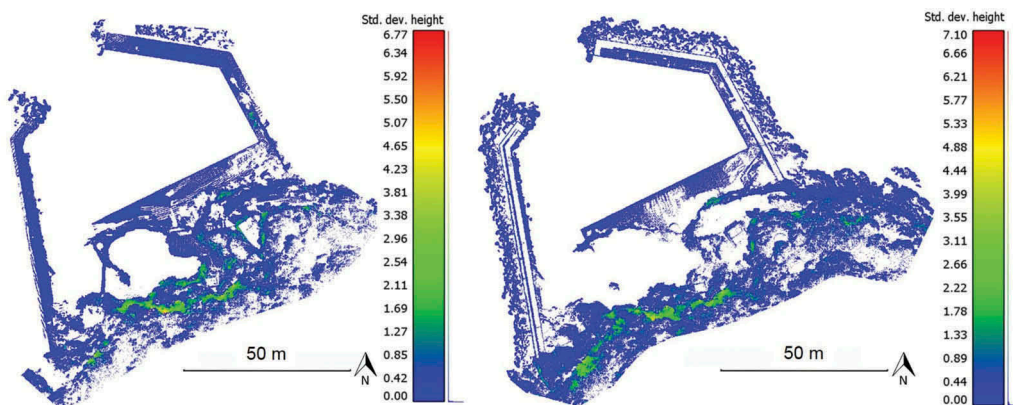

Figure 9. Standard deviation height for static (left) and kinematic (right) DSMs.
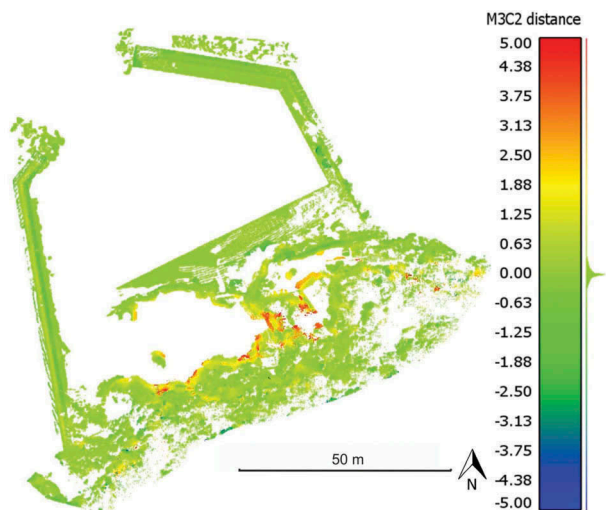

Figure 10. Difference between static and kinematic DSMs heights (static – kinematic), and statistical distribution of the values (next to the scale bars).

The same criterion of comparing the DSMs over different surfaces has been also applied concerning the "horizontal" differences between the two point clouds. In this case, the DSMs have been computed defining a grid on a convenient plane parallel to the vertical axis. The clouds have been oriented to face the North-South direction orthogonally, to guarantee the correct projection of the points in the DSMs cells.

The same areas depicted in Figure 11 have been considered to compute the DSMs, but taking into account only a sample of the East pier, considered representative of the entire structure. Figure 12 depicts the front view of each portion; A, B and C represent the point of views.

Then, the so-obtained DSMs for the static and kinematic survey have been compared to compute their differences. The resulting difference clouds are reported in Figure 13 and the average values and standard deviations are listed in Table 4. The average

Table 3. Average values and standard deviations for the considered portions of DSM.

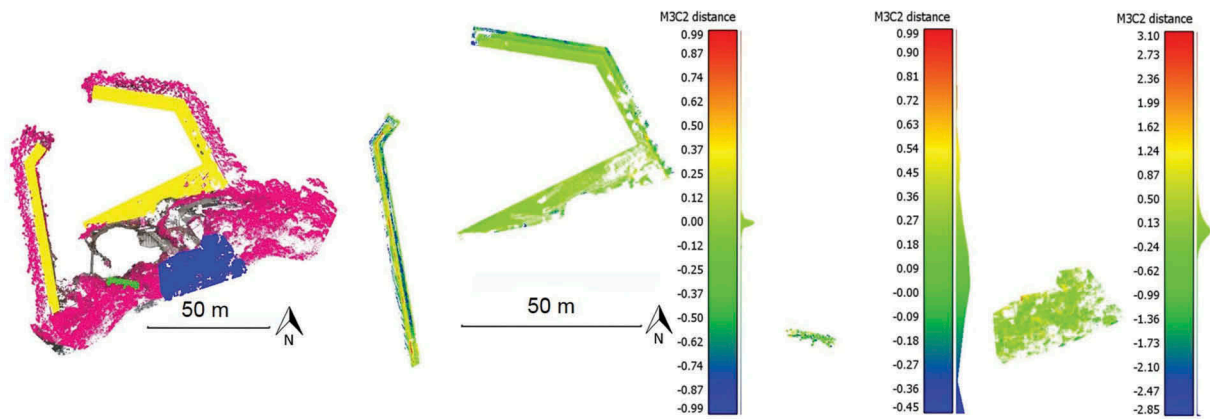| Portion	Differences average value [m]	Differences standard deviation [m]
Piers and dock	−0.1	0.33
Cliff	0.13	0.25
Vegetated area	0.12	0.43

Figure 11. Different portions of the point clouds considered for the comparison: on the left, the positions of the dock and piers (yellow), the rocky cliff (green) and the vegetated area (blue). From the center to the right, the difference (static – kinematic) in heights, and statistical distribution of the values (next to the scale bars) for the three areas.
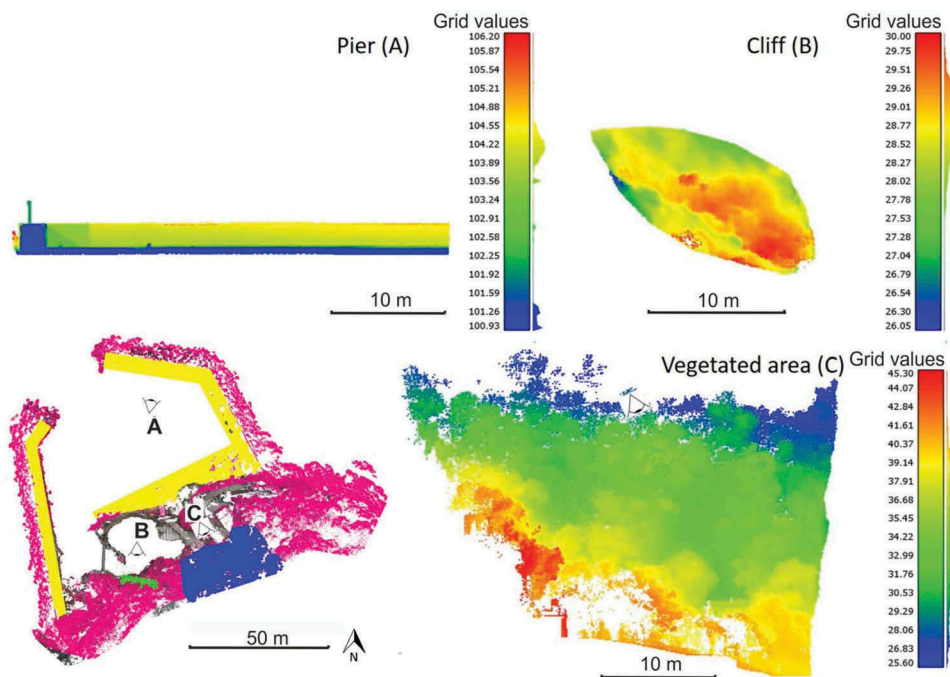

Figure 12. DSMs for pier, cliff and vegetated area as seen from their point-views (A, B, C).

values of differences are limited for both the cliff and vegetated area, while the standard deviation of vegetated area is higher than the cliff one, as expected from the configuration of the point clouds. The high average value of the pier is due to the bad representation of the vertical wall of the pier in the kinematic survey (the yellow areas in the top left part of Figure 13); excluding those portions, the average value and standard deviation are 0.07 m and 0.19 m, respectively.

The point cloud noise, represented by the heights standard deviation of the points inside each cell of the DSM, has been also quantified for one of the SCMR (Sea Cliff Mass Rating) test areas (point 4 in Figure 5), surveyed only in kinematic mode. The sample on the West side of the promontory has been chosen because it is partly covered by vegetation and partly bare rock; this

characteristic leads to an interesting "internal" comparison between the two surfaces (vegetated and rock).

Again, the DMS has been computed on a 10×10 cm grid defined on a plane parallel to the vertical axis, orthogonally facing the North-South direction. Figure 14 represents a perspective view of the DSM and its standard deviation height, i.e. the point cloud noise.

The point cloud noise is almost uniform over the vegetated and the bare rock areas. The higher values on the right portion of the cliff do not depend on the type of surface, but seem more related to the kinematic survey acquisition geometry and to the rock layers orientation.

The average value and standard deviation of point cloud noise in the considered sample are 0.07 m and 0.19 m, respectively. They have a similar order of
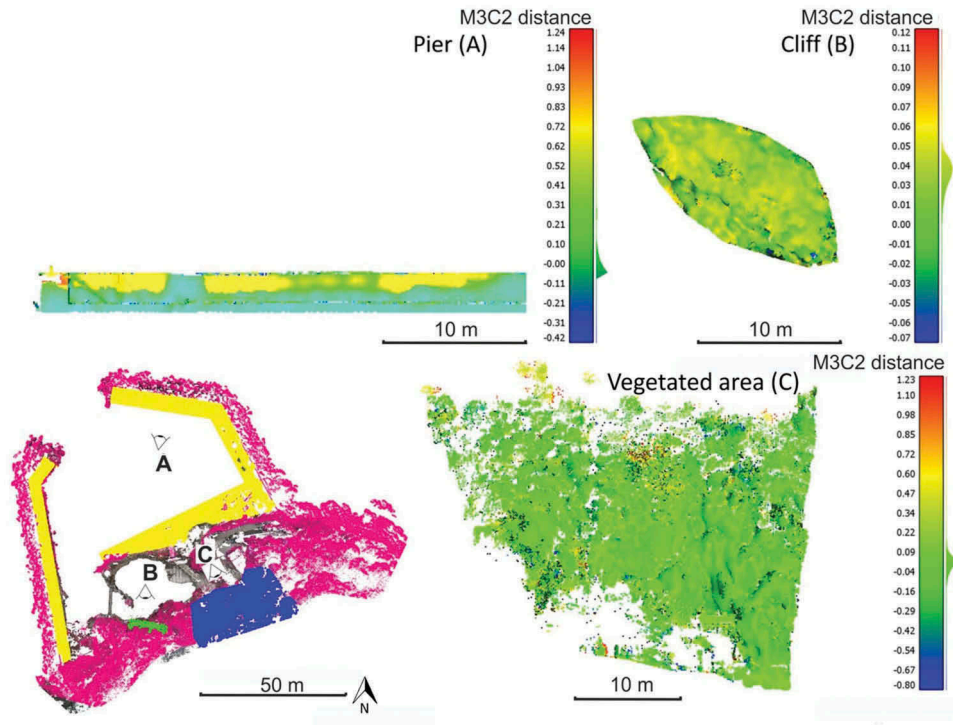
Figure 13. "Horizontal" differences (static – kinematic), and statistical distribution of the values (next to the scale bars) for the three areas.

magnitude of average value and standard deviation of the kinematic survey of the refuge port (0.1 m and 0.19 m, respectively), having excluded the vegetated area. This confirms the good quality of the kinematic survey, which could be successfully used as an integration of a static survey, or even substitute it when it is necessary to access unsafe or unreachable places, where a static survey is not suitable.

Table 4. Average values and standard deviations for the considered portions of DSMs.

Portion	Differences average value	Differences standard deviation
	[m]	[m]
Pier	0.17	0.32
Cliff	0.03	0.05
Vegetated area	0.04	0.27

Geomorphological susceptibility mapping

Considering the effectiveness of the configuration adopted during the acquisition, MBES and LS have been correctly aligned and integrated, in order to reconstruct the morphology of the Gallinara Island at high detail. Sea beds multibeam data allowed to obtain a detailed grid of 0.25×0.25 m of the submerged area, while emerged rocky coast were described at 2–4 cm of resolution by laser scanner data (Figure 15).

The 3D digital model of both emerged and submerged areas was reliable and useful for geomorphological observation and geo-structural analysis. Based on DSM data, together with field survey from the boat and aerial photo interpretation, geomorphological features of the island have been outlined.

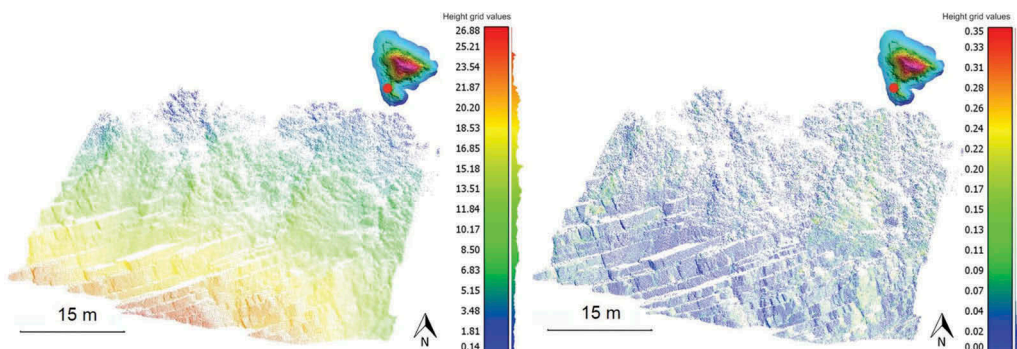The whole perimeter of the island is almost totally characterized by active rocky cliff, made up of

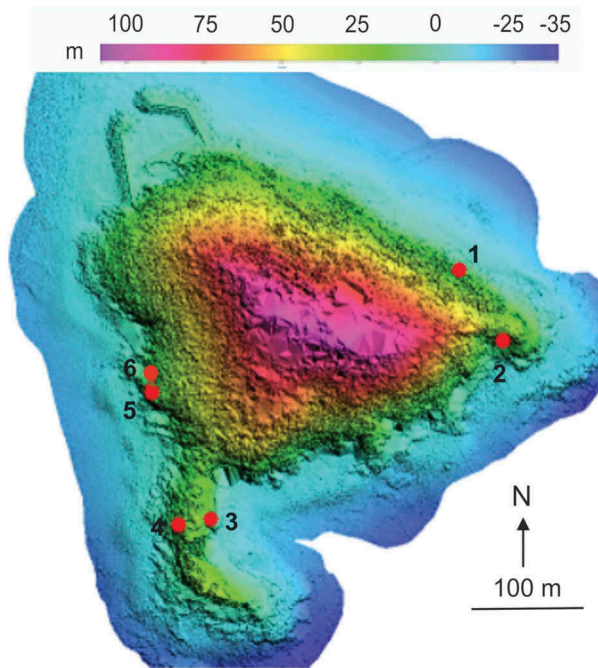**Figure 14.** DSM (left) and standard deviation height (right).

Figure 15. Gallinara Island DSM of emerged-submerged areas, obtained by the integration of LS and MBES techniques. The red dots indicate the location of the stations used for the application of SCMR.

quartzites in the southern and north-western sectors of the islands and of conglomerates in the western sector, with heights up to 30 m. An active rock fall coastal landslide has been mapped along the southern sector of the island, affected by dominant wave motion from SW and secondary from SE. Two almost flat surfaces, identifiable as relict quaternary marine terraces, are observable on the eastern and western promontories at an elevation of about 30–32 m a.s.l.

In this area, waves come predominantly from the South (Cattaneo Vietti et al., 2010; Ferrari, Bolens, Bozzano, Fierro, & Gentile, 2006). Waves coming from South–West are the most intense and frequent ($H_s = 7.8$ m), followed by waves from the South–East ($H_s = 4.0$ m), which, although less intense than waves from South, are comparatively more frequent, referring to 50 years recurrence times (Regione Liguria, 2013). SCMR classification was carried out in six representative areas of the island, identified as red dots in Figure 15. Surveys, made on approximately 50 m for each area, highlighted the quality of the rocky cliff in relation to bedrock condition and sea wave action as shown in Figure 16 and synthesized in Table 5.

The correlation between SCMR and geomorphological data allowed to produce the rock-failure susceptibility map of the island perimeter. Very high susceptibility (SCI-4) has been found in the southern sector of the island within a wider sector with medium susceptibility (SCI-2). The remaining sea cliffs are classified between very low (SCI-0) and low (SCI-1) susceptibility, except for a small sector affected by an active rock fall (Figure 17), which is characterized by high susceptibility (SCI-3).

Discussion and conclusion

The integration between multibeam and laser scanner techniques, experienced along the rocky coast of the Gallinara Island (Western Liguria, Italy), leads to
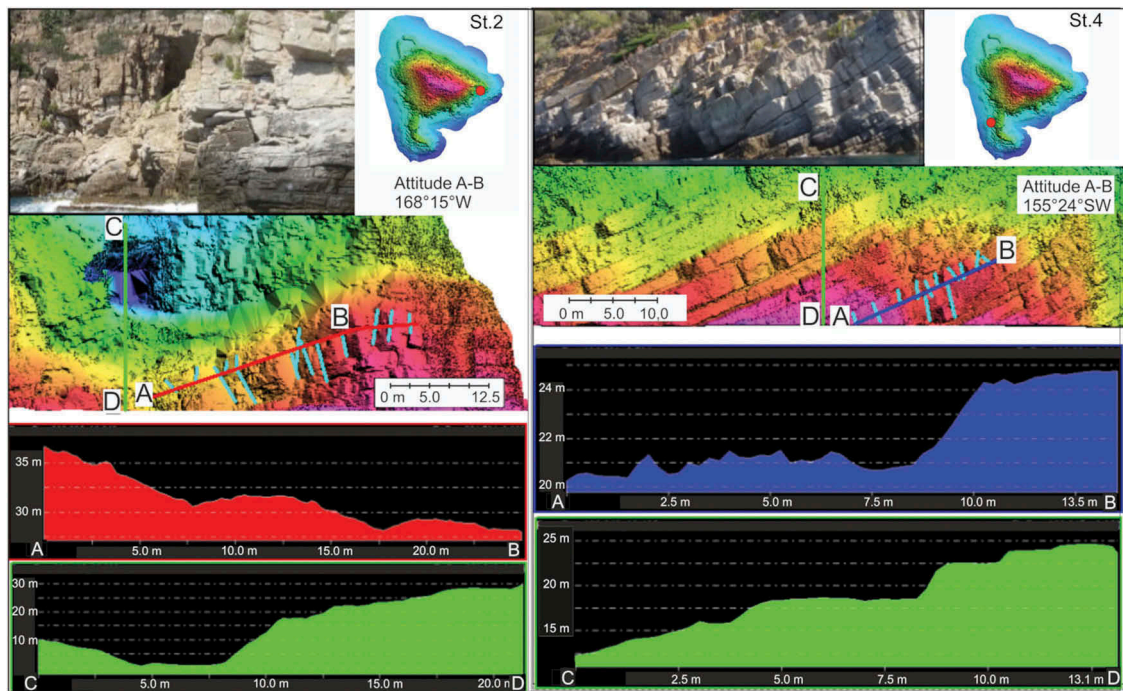

Figure 16. Rocky cliff conditions in the Eastern sector (station 2) and in the western sector (station 4) characterized by outcrops of quartzites detected by the laser scanner technique. For stations locations, see Figure 15.

Table 5. Application of SCMR Classification in six representative sectors of Gallinara Island rocky cliff condition. For the location of the test areas see Figure 15.

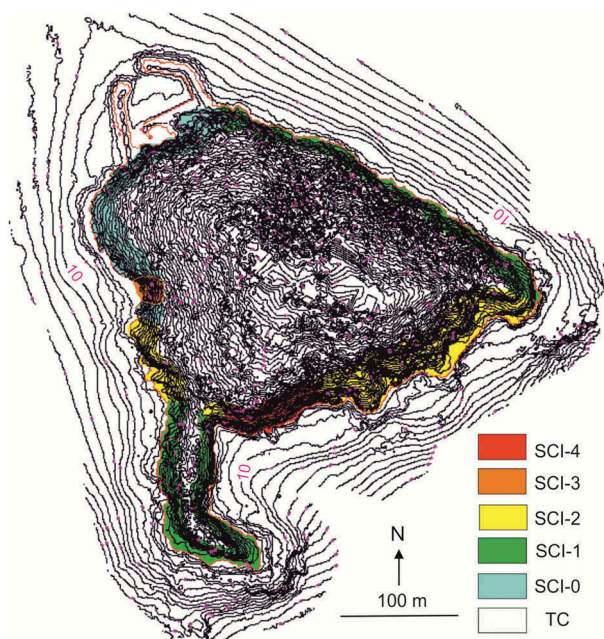| PARAMETER/SCMR VALUE	STATION					
	1	2	3	4	5	6
Lithotype	Quartzites	Quartzites	Quartzites	Quartzites	Quartzites	Conglomerates
- UCS of intact rock material	> 250 MPa	> 250 MPa	> 250 MPa	> 250 MPa	> 250 MPa	25 -50 MPa
R1	15	15	15	15	15	4
RQD (%)	50 – 75	50 – 75	25 – 50	50 – 75	50 – 75	90 – 100
R2	13	13	8	13	13	20
Spacing between discontinuities	0.6 – 2 m	> 2 m	> 2 m	> 2 m	0.6 – 2 m	-
R3	15	20	20	20	15	15
Persistence of discontinuities	1 – 3 m	< 1 m	< 1 m	< 1 m	< 1 m	none
R4	4	6	6	6	6	6
Aperture of discontinuities	> 5 mm	> 5 mm	> 5 mm	> 5 mm	> 5 mm	none
R4	0	0	0	0	0	6
Roughness of discontinuity surfaces	slightly rough	slightly rough	slightly rough	slightly rough	slightly rough	none
R4	3	3	3	3	3	6
Infilling material	soft filling < 5 mm	soft filling < 5 mm	soft filling < 5 mm	soft filling < 5 mm	soft filling < 5 mm	none -
R4	2	2	2	2	2	6
Weathering of joint walls	highly weathered	highly weathered	highly weathered	highly weathered	highly weathered	none
R4	1	1	1	1	1	6
Hydraulic condition	wet	wet	wet	highly weathered	wet	damp
R5	7	7	7	1	7	10
FACTOR FOR JOINT	**RANGE OF VALUE**					
Plane/wedge failure $|\alpha j-\alpha f|$ Toppling $|\alpha j-\alpha f-180|$	> 30°	> 30°	> 30°	> 30°	> 30°	-
F1	0.15	0.15	0.15	0.15	0.15	-
Plane/wedge failure (βj)	> 45°	> 45°	30° – 35°	> 45°	> 45°	-
F2 plane/wedge	1	1	0.7	1	1	-
Plane/wedge failure ($\beta j-\beta f$)	> 10°	> 10°	> 10°	0°	0°	-
Toppling ($\beta j+\beta f$)	< 110°	< 110°	< 110°	> 120°	> 120°	-
F3	0	0	0	-25	-25	-
Sea cliff conditions	natural slope	natural slope	natural slope	natural slope	natural slope	natural slope
F4$_m$	15	15	15	15	15	15
WAVE MOTION	**RANGE OF VALUE**					
Wave energy	Broken waves E < 30	Breaking waves 15<E<30	Breaking waves E > 30	Breaking waves E > 30	Breaking waves E > 30	Breaking waves E > 30
M1	1	6	8	8	8	8
Cliff angle α	0 – 30	30 – 55	30 – 55	30 – 55	70 – 90	30 – 55
M2	0	1	1	1	5	1
θ wave motion	25-50	25-50	90	25-50	25-50	25-50
M3	3	3	10	3	3	3
SCMR VALUE	74	72	58	66	57	82
SCMR CLASS	II	II	III	II	III	I

Figure 17. Susceptibility Coastal Instability (SCI) map: SCI-4 – very high susceptibility – active landslides and sea cliffs with SCMR = 0–20; SCI-3 – high susceptibility – deep seated gravitational slope deformation (D.S.G.S.D.) and sea cliffs with SCMR = 21–40; SCI-2 – medium susceptibility – sea cliffs with SCMR = 41–60; SCI-1 – low susceptibility – sea cliffs with SCMR = 61–80; SCI-0 – very low susceptibility – beaches and sea cliffs with SCMR = 81–100; TC – techno-coast (Isobath equidistance 2 m).

interesting results. Multibeam data allowed to reconstruct the submerged area with a detailed grid of 0.25 × 0.25 m, while a laser scanner allowed to describe the emerged rocky coast morphology at high resolution (2–4 cm). Such high resolution was requested by geomorphological analysis addressed to evaluate sea cliff instability, as prescribed by coastal hazard and risk mitigation measures (Brandolini, Faccini, Robbiano, & Terranova, 2007, 2013; Esposito, Salvini, Matano, Sacchi, & Troise, 2018; Matano et al., 2016; Rosser et al., 2005).

Focusing on the accuracy of the reconstructed 3D surfaces, it was interesting to verify the quality of laser scanner used as profiler from the boat, being the multibeam survey a consolidated technique widely applied under water (Clarke, Mayer, & Wells, 1996; Monteys et al., 2015). The comparison between static and kinematic laser scanner surveys in the refuge port of Gallinara Island allowed to estimate an average difference and a standard deviation lower than 5 cm of the kinematic DSM with respect to the static and more precise one on rocky cliffss. Vegetated areas are obviously characterized by higher noise. Thanks to its good quality, the kinematic laser scanner survey was successfully used outside the refuge port, along the rocky cliffs of the island, where a static survey was not suitable (Alho et al., 2009; Boeder et al., 2010).

The resulting DTMs, derived by the integration of multibeam and laser scanner point clouds, allowed to obtain significative geological and geomorphological information useful for the evaluation of rocky cliffs conditions and for mapping rock-failure susceptibility (De Vita et al., 2012).

In conclusion, the integrated remote sensing technologies have proven to be very effective both in terms of time, cost and accuracy of the results. The integrated survey based on MBES and LS techniques allowed to detect a large amount of high-accuracy and significant data in a single survey campaign, even in areas which are difficult to detect with direct traditional techniques. The results allowed to consistently assess the stability conditions of rocky coast, indicating the South-Western sectors of Gallinara Island as the most hazardous areas, due to their exposure to dominant waves from the South.

Disclosure statement

No potential conflict of interest was reported by the authors.

ORCID

Bianca Federici http://orcid.org/0000-0002-4598-4758
Nicola Corradi http://orcid.org/0000-0003-1125-7197
Ilaria Ferrando http://orcid.org/0000-0002-9121-6821
Domenico Sguerso http://orcid.org/0000-0001-7683-3306
Pierluigi Brandolini http://orcid.org/0000-0002-4009-6188

References

Aguilar, F. J., Fernandez, I., Casanova, J. A., Ramos, F. J., Aguilar, M. A., Blanco, J. L., & Moreno, J. C. (2017). 3D Coastal Monitoring from very dense UAV-Based Photogrammetric Point Clouds. In: Eynard B., Nigrelli V., Oliveri S., Peris-Fajarnes G., Rizzuti S. (eds) *Advances on Mechanics, Design Engineering and Manufacturing. Lecture Notes in Mechanical Engineering* (pp. 879–887). Cham: Springer.

Alho, P., Kukko, A., Hyyppä, H., Kaartinen, H., Hyyppä, J., & Jaakkola, A. (2009). Application of boat-based laser scanning for river survey. *Earth Surface Processes and Landforms: the Journal of the British Geomorphological Research Group*, 34(13), 1831–1838. doi:10.1002/esp. v34:13

Bieniawski, Z.T. (1989). *Engineering rock mass classifications: A complete manual for engineers and geologists in mining, civil, and petroleum engineering.* John Wiley & Sons

Boeder, V., Kersten, T.P., Hesse, C., Thies, T., & Sauer, A. (2010). Initial experience with the integration of a terrestrial laser scanner into the mobile hydrographic multi sensor system on a ship. ISPRS Istanbul Workshop 2010, WG I/4Modeling of optical airborne and space borne sensorsIstanbul, Turkey, October 11 – 13, 2010 .

Brandolini, P., & Cevasco, A. (2015). Geo-hydrological risk mitigation measures and land-management in a highly vulnerable small coastal catchment. In Engineering Geology for Society and Territory, Volume 5 (pp. 759–762). Editors: Giorgio Lollino, Andrea Manconi, Fausto Guzzetti, Martin Culshaw, Peter Bobrowsky, Fabio Luino. Switzerland: Springer International Publishing. doi: 10.1007/978-3-319-09048-1_147.

Brandolini, P., Faccini, F., Pelfini, M., & Firpo, M. (2013). A complex landslide along the Eastern Liguria rocky coast (Italy). *Rendiconti Online Società Geologica Italiana*, *28*, 28–31.

Brandolini, P., Faccini, F., Robbiano, A., & Terranova, R. (2007). Geomorphological hazards and monitoring activity along the western rocky coast of the Portofino Promontory (Italy). *Quaternary International*, *171*, 131–142. doi:10.1016/j.quaint.2006.11.006

Brandolini, P., Faccini, F., Robbiano, A., & Terranova, R. (2009). Slope instability on rocky coast: A case study of Le Grazie landslides (eastern Liguria. *Northern italy*). *Geological Society, London, Special Publications*, *322*(1), 143–154. doi:10.1144/SP322.6

Brandolini, P., Pepe, G., Capolongo, D., Cappadonia, C., Cevasco, A., Conoscenti, C., ... Del Monte, M. (2018). Hillslope degradation in representative Italian areas: Just soil erosion risk or opportunity for development? *Land Degradation & Development*, *29*(9), 3050–3068. doi:10.1002/ldr.v29.9

Brennan, C.W. (2009). R2Sonic LL Multibeam Training – Multibeam Surveying ©2009 R2Sonic LL.

Campobasso, C., Carton, A., Chelli, A., D'Orefice, M., Dramis, F., Graciotti, R., ... Pellegrini, L. (2018). Aggiornamento ed integrazioni delle Linee guida della Carta geomorfologica d'Italia alla scala 1:50.000. Progetto CARG: modifiche ed integrazioni al Quaderno n. 4/1994. Quaderni serie III 13 (1).

Caputo, T., Marino, E., Matano, F., Somma, R., Troise, C., & De Natale, G. (2018). Terrestrial Laser Scanning (TLS) data for the analysis of coastal tuff cliff retreat: Application to Coroglio cliff, Naples, Italy. *Annals of Geophysics*, *61*(1), 110. doi:10.4401/ag-7494

Cattaneo Vietti, R., Albertelli, G., Aliani, S., Bava, S., Bavestrello, G., Cecchi, L.B., ... Wurtz, M. (2010). The Ligurian Sea: Present status, problems and perspectives. *Chemistry and Ecology*, *26*(S1), 319–340. doi:10.1080/02757541003689845

Cevasco, A., Pepe, G., & Brandolini, P. (2013). Geotechnical and stratigraphic aspects of shallow landslides at Cinque Terre (Liguria, Italy). *Rendiconti Online Società Geologica Italiana*, *24*, 52–54.

Chelli, A., Aringoli, D., Aucelli, P.P., Baldassarre, M.A., Bellotti, P., Bini, M., ... Valente, A. (2018). Morphodynamics of coastal areas represented in the new geomorphologic map of Italy: Draw the landforms of the past to outline the future. *Alpine and Mediterranean Quaternary*, *31*(1), 17–21.

Clarke, J.E.H., Mayer, L.A., & Wells, D.E. (1996). Shallow-water imaging multibeam sonars: A new tool for investigating seafloor processes in the coastal zone and on the continental shelf. *Marine Geophysical Researches*, *18*(6), 607–629. doi:10.1007/BF00313877

CloudCompare (version 2.10.1) [GPL software]. (2019). Retrieved from http://www.cloudcompare.org/

Colbo, K., Ross, T., Brown, C., & Weber, T. (2014). A review of oceanographic applications of water column data from multibeam echosounders. *Estuarine, Coastal and Shelf Science*, *145*, 41–56. doi:10.1016/j.ecss.2014.04.002

De Vita, P., Cevasco, A., & Cavallo, C. (2012). Detailed rock failure susceptibility mapping in steep rocky coasts by means of non-contact geostructural surveys: The case study of the Tigullio Gulf (Eastern Liguria, Northern Italy). *Natural Hazards and Earth System Sciences*, *12* (4), 867. doi:10.5194/nhess-12-867-2012

Del Monte M., E., Vergari, Brandolini P., Capolongo D., Cevasco A., Ciccacci S., Conoscenti C., Fredi P., Melelli L., Rotigliano F., Zucca F. (2014). *Multi-method evaluation of denudation rates in small Mediterranean catchments*. In: G. Lollino et al. (eds.), Engineering Geology for Society and Territory – Volume 1, pp. 1-5, doi:10.1007/978-3-319-09300-0_105, © Springer International Publishing Switzerland 2014.

Esposito, G., Salvini, R., Matano, F., Sacchi, M., & Troise, C. (2018). Evaluation of geomorphic changes and retreat rates of a coastal pyroclastic cliff in the Campi Flegrei volcanic district, southern Italy. *Journal of Coastal Conservation*, *22*(5), 957–972. doi:10.1007/s11852-018-0621-1

Faccini, F., Brandolini, P., Robbiano, A., Perasso, L., & Sola, A. (2005). Fenomeni di dissesto e precipitazioni in rapporto alla pianificazione territoriale: L'evento alluvionale del novembre 2002 nella bassa val Lavagna (Liguria orientale) [Instability, precipitation phenomena and land planning: The flood of 2002 in lower Lavagna valley (Eastern Liguria, Italy)]. *Geografia Fisica e Dinamamica Quaternaria*, *Suppl 7*, 145–153.

Ferrari, M., Bolens, S., Bozzano, A., Fierro, G., & Gentile, R. (2006). The port of Genoa-Voltri (Liguria, Italy): A case of updrift erosion. *Chemistry and Ecology*, *22*(sup1), S361–S369. doi:10.1080/02757540600688051

Ferrari, M., Carpi, L., Pepe, G., Mucerino, L., Schiaffino, C. F., Brignone, M., & Cevasco, A. (2019). A geomorphological and hydrodynamic approach for beach safety and sea bathing risk estimation. *Science of the Total Environment*, *671*, 1214–1226. doi:10.1016/j.scitotenv.2019.03.378

Gagliolo, S., Fagandini, R., Passoni, D., Federici, B., Ferrando, I., Pagliari, D., ... Sguerso, D. (2018). Parameter optimization for creating reliable photogrammetric models in emergency scenarios. *Applied Geomatics*, *10*(4), 501–514. doi:10.1007/s12518-018-0224-4

Guida, S., Corradi, N., Federici, B., Lucarelli, A., & Brandolini, P. (2019). Laser scanner and multibeam integrated survey for the assessment of rocky sea cliff geomorphological hazard. In G. Chirici & M. Gianinetto (Eds.), *Earth observation advancements in a changing world, Trends in Earth Observation, AIT Series, 1* (pp. 162–166). doi:10.978.88944687/17

Lague, D., Brodu, N., & Leroux, J. (2013). Accurate 3D comparison of complex topography with terrestrial laser scanner: Application to the Rangitikei canyon (N-Z). *ISPRS Journal of Photogrammetry and Remote Sensing*, *82*, 10–26. doi:10.1016/j.isprsjprs.2013.04.009

Lucchetti, A., Brandolini, P., Faccini, F., & Firpo, M. (2014). Proposta di valutazione della stabilità delle coste rocciose (SCMR–Sea Cliff Mass Rating): Il caso studio delle falesie tra Genova e Camogli (Liguria orientale) [Proposal of evaluation of rocky coast stability (SCMR – Sea Cliff Mass Rating): The case study of the cliffs between Genoa and Camogli (Eastern Liguria)]. *Studi Costieri*, *22*, 137–149.

Mancini, F., Dubbini, M., Gattelli, M., Stecchi, F., Fabbri, S., & Gabbianelli, G. (2013). Using unmanned aerial vehicles (UAV) for high-resolution reconstruction of topography:

The structure from motion approach on coastal environments. *Remote Sensing*, 5(12), 6880–6898. doi:10.3390/rs5126880

Mastronuzzi, G., Aringoli, D., Aucelli, P.P., Baldassarre, M. A., Bellotti, P., Bini, M., … Valente, A. (2017). The geomorphological map of the Italian coast: From a descriptive to a morphodynamic approach. *Geografia Fisica E Dinamica Quaternaria*, 40, 1–36.

Matano, F., Iuliano, S., Somma, R., Marino, E., Del Vecchio, U., Esposito, G., … Sacchi, M. (2016). Geostructure of Coroglio tuff cliff, Naples (Italy) derived from terrestrial laser scanner data. *Journal of Maps*, 12(3), 407–421. doi:10.1080/17445647.2015.1028237

Mills, J.P., Buckley, S.J., Mitchell, H.L., Clarke, P.J., & Edwards, S.J. (2005). A geomatics data integration technique for coastal change monitoring. *Earth Surface Processes and Landforms: the Journal of the British Geomorphological Research Group*, 30(6), 651–664. doi:10.1002/(ISSN)1096-9837

Monteys, X., Harris, P., Caloca, S., & Cahalane, C. (2015). Spatial prediction of coastal bathymetry based on multispectral satellite imagery and multibeam data. *Remote Sensing*, 7(10), 13782–13806. doi:10.3390/rs71013782

Naylor, L.A., Stephenson, W.J., & Trenhaile, A.S. (2010). Rock coast geomorphology: Recent advances and future research directions. *Geomorphology*, 114(1–2), 3–11. doi:10.1016/j.geomorph.2009.02.004

Nex, F., & Remondino, F. (2014). UAV for 3D mapping applications: A review. *Applied Geomatics*, 6(1), 1–15. doi:10.1007/s12518-013-0120-x

Passoni, D., Federici, B., Ferrando, I., Gagliolo, S., & Sguerso, D. (2018). The estimation of precision in the planning of UAS photogrammetric surveys. International Archives of the Photogrammetry. *Remote Sensing and Spatial Information Sciences*, 42(2), 837–843.

Pranzini, E., & Williams, A. (2013). *Coastal erosion and protection in Europe* (pp. 488). London: Routeledge. eISBN: 9781136469862.

Raso, E., Brandolini, P., Faccini, F., & Firpo, M. (2016). The Guvano complex landslide in the Cinque Terre National Park. In *ISRM International Symposium-EUROCK 2016. International Society for Rock Mechanics and Rock Engineering*. Italy: Geomorphological characterization, GNSS monitoring and risk management.

Raso, E., Brandolini, P., Faccini, F., Realini, E., Caldera, S., & Firpo, M. (2017). Geomorphological evolution and monitoring of San Bernardino-Guvano coastal landslide (Eastern Liguria, Italy). *Geografia Fisica E Dinamica Quaternaria*, 40(2), 197–210.

Regione Liguria. (2013). Piano di tutela dell'ambiente marino e costiero. Ambito costiero 08, Unità fisiografiche del Centa, Centa sud e Maremola. Retrieved from http://www.ambienteinliguria.it/lirgw/eco3/ep/linkPagina.do?canale=/Home/030acque/030mare costm/010competenzeRLacquemarine/040pianotutelaambientemarinocostiero

RIEGL GmbH. (2010). Long range & high accuracy 3D terrestrial laser scanner. Retrieved from http://www.riegl.com/uploads/tx_pxpriegldownloads/10_DataSheet_Z420i_03-05-2010.pdf

Romana, M.R. (1993). A geomechanical classification for slopes: Slope mass rating. In: *Comprehensive rock engineering*, vol 3, Pergamon, UK, Hudson JA (ed), pp. 575–600.

Rosser, N.J., Petley, D.N., Lim, M., Dunning, S.A., & Allison, R.J. (2005). Terrestrial laser scanning for monitoring the process of hard rock coastal cliff erosion. *Quarterly Journal of Engineering Geology and Hydrogeology*, 38(4), 363–375. doi:10.1144/1470-9236/05-008

Scarpati, A., Pepe, G., Mucerino, L., Brandolini, P., & Firpo, M. (2013). Rocky cliff landslide hazard: The Capo Noli Promontory case study (western Liguria, NW Mediterranean Sea). *Rendiconti Online Società Geologica Italiana*, 28, 137–141.

Troisi, S., Del Pizzo, S., Gaglione, S., Miccio, A., & Testa, R.L. (2015). 3D models comparison of complex shell in underwater and dry environments. *The International Archives of Photogrammetry, Remote Sensing and Spatial Information Sciences*, 40(5), 215. doi:10.5194/isprsarchives-XL-5-W5-215-2015